ARTICLE

Bi-allelic Variants in *TONSL* Cause SPONASTRIME Dysplasia and a Spectrum of Skeletal Dysplasia Phenotypes

Lindsay C. Burrage,[1,2,39] John J. Reynolds,[3,39] Nissan Vida Baratang,[4] Jennifer B. Phillips,[5] Jeremy Wegner,[5] Ashley McFarquhar,[4] Martin R. Higgs,[3] Audrey E. Christiansen,[6] Denise G. Lanza,[1] John R. Seavitt,[1] Mahim Jain,[7] Xiaohui Li,[1] David A. Parry,[8] Vandana Raman,[9] David Chitayat,[10,11] Ivan K. Chinn,[12,13] Alison A. Bertuch,[1] Lefkothea Karaviti,[14] Alan E. Schlesinger,[15,16] Dawn Earl,[17] Michael Bamshad,[17,18] Ravi Savarirayan,[19] Harsha Doddapaneni,[20] Donna Muzny,[20] Shalini N. Jhangiani,[20] Christine M. Eng,[1,21] Richard A. Gibbs,[1,20] Weimin Bi,[1,21] Lisa Emrick,[1,12,22] Jill A. Rosenfeld,[1] John Postlethwait,[5] Monte Westerfield,[5] Mary E. Dickinson,[1,6] Arthur L. Beaudet,[1] Emmanuelle Ranza,[23] Celine Huber,[24] Valérie Cormier-Daire,[24] Wei Shen,[25,26] Rong Mao,[25,26] Jason D. Heaney,[1] Jordan S. Orange,[13,27] University of Washington Center for Mendelian Genomics, Undiagnosed Diseases Network, Débora Bertola,[28,29] Guilherme L. Yamamoto,[28,29]

(Author list continued on next page)

SPONASTRIME dysplasia is an autosomal-recessive spondyloepimetaphyseal dysplasia characterized by spine (spondylar) abnormalities, midface hypoplasia with a depressed nasal bridge, metaphyseal striations, and disproportionate short stature. Scoliosis, coxa vara, childhood cataracts, short dental roots, and hypogammaglobulinemia have also been reported in this disorder. Although an autosomal-recessive inheritance pattern has been hypothesized, pathogenic variants in a specific gene have not been discovered in individuals with SPONASTRIME dysplasia. Here, we identified bi-allelic variants in *TONSL*, which encodes the Tonsoku-like DNA repair protein, in nine subjects (from eight families) with SPONASTRIME dysplasia, and four subjects (from three families) with short stature of varied severity and spondylometaphyseal dysplasia with or without immunologic and hematologic abnormalities, but no definitive metaphyseal striations at diagnosis. The finding of early embryonic lethality in a *Tonsl*$^{-/-}$ murine model and the discovery of reduced length, spinal abnormalities, reduced numbers of neutrophils, and early lethality in a *tonsl*$^{-/-}$ zebrafish model both support the hypomorphic nature of the identified *TONSL* variants. Moreover, functional studies revealed increased amounts of spontaneous replication fork stalling and chromosomal aberrations, as well as fewer camptothecin (CPT)-induced RAD51 foci in subject-derived cell lines. Importantly, these cellular defects were rescued upon re-expression of wild-type (WT) *TONSL*; this rescue is consistent with the hypothesis that hypomorphic *TONSL* variants are pathogenic. Overall, our studies in humans, mice, zebrafish, and subject-derived cell lines confirm that pathogenic variants in *TONSL* impair DNA replication and homologous recombination-dependent repair processes, and they lead to a spectrum of skeletal dysplasia phenotypes with numerous extra-skeletal manifestations.

Introduction

SPONASTRIME dysplasia (MIM: 271510) is an autosomal-recessive spondyloepimetaphyseal dysplasia named for characteristic clinical and radiographic findings, including spine (spondylar) abnormalities, midface hypoplasia with a depressed nasal bridge, and striation of the metaphyses.[1] Additional features include disproportionate short stature with exaggerated lumbar lordosis, scoliosis, coxa vara, limited elbow extension, childhood cataracts, short

[1]Department of Molecular and Human Genetics, Baylor College of Medicine, Houston, TX 77030, USA; [2]Texas Children's Hospital, Houston, TX 77030, USA; [3]Institute of Cancer and Genomic Sciences, University of Birmingham, Birmingham B15 2TT, UK; [4]Centre Hospitalier Universitaire Sainte-Justine Research Center, University of Montreal, Montreal, QC H3T1J4, Canada; [5]Institute of Neuroscience, University of Oregon, Eugene, OR 97403, USA; [6]Department of Molecular Physiology and Biophysics, Baylor College of Medicine, Houston, TX 77030, USA; [7]Department of Bone and Osteogenesis Imperfecta, Kennedy Krieger Institute, Baltimore, MD 21205, USA; [8]Medical Research Council Institute of Genetics & Molecular Medicine, the University of Edinburgh, Western General Hospital, Crewe Road, Edinburgh EH4 2XU, UK; [9]Division of Pediatric Endocrinology and Diabetes, University of Utah, Salt Lake City, UT 84112, USA; [10]The Prenatal Diagnosis and Medical Genetics Program, Department of Obstetrics and Gynecology, Mount Sinai Hospital, University of Toronto, Toronto, ON M5G 1Z5, Canada; [11]Department of Pediatrics, Division of Clinical and Metabolic Genetics, the Hospital for Sick Children, University of Toronto, Toronto, ON M5G 1X8, Canada; [12]Department of Pediatrics, Baylor College of Medicine, Houston, TX 77030, USA; [13]Division of Pediatric Immunology, Allergy, and Rheumatology, Texas Children's Hospital, Houston, TX 77030, USA; [14]Division of Diabetes and Endocrinology, Texas Children's Hospital, Houston, TX 77030, USA; [15]Department of Pediatric Radiology, Texas Children's Hospital, Houston, TX 77030, USA; [16]Department of Radiology, Baylor College of Medicine, Houston, TX 77030, USA; [17]Seattle Children's Hospital, Seattle, WA 98195, USA; [18]Departments of Pediatrics and Genome Sciences, University of Washington, Seattle, WA 98195, USA; [19]Victorian Clinical Genetics Services, Murdoch Children's Research Institute, University of Melbourne, Parkville, VIC 3052, Australia; [20]Human Genome Sequencing Center, Baylor College of Medicine, Houston, TX 77030, USA; [21]Baylor Genetics, Houston, TX 77030, USA; [22]Division of Neurology and Developmental Neuroscience and Department of Pediatrics, Baylor College of Medicine, Houston, TX 77030, USA; [23]Service of Genetic Medicine, University of Geneva Medical School, Geneva University Hospitals, 1205 Geneva, Switzerland; [24]Department of Genetics, INSERM UMR1163, Université Paris Descartes-Sorbonne Paris Cité, Institut Imagine, AP-HP, Hôpital Necker Enfants Malades, Paris 75015, France; [25]Associated Regional and University Pathologists Laboratories, Salt Lake City, UT 84108, USA; [26]Department of Pathology, University of Utah, Salt Lake City, UT 84112, USA; [27]Current affiliation: Department of Pediatrics, Columbia University Vagelos College of Physicians and Surgeons,

(Affiliations continued on next page)

Wagner A.R. Baratela,[28] Merlin G. Butler,[30] Asim Ali,[31] Mehdi Adeli,[32] Daniel H. Cohn,[33] Deborah Krakow,[34] Andrew P. Jackson,[35] Melissa Lees,[36] Amaka C. Offiah,[37] Colleen M. Carlston,[25,26] John C. Carey,[38] Grant S. Stewart,[3,40] Carlos A. Bacino,[1,2,40] Philippe M. Campeau,[4,40] and Brendan Lee[1,2,40,*]

dental roots, and hypogammaglobulinemia[2–9]. Radiographically, the abnormalities of the lumbar vertebral bodies are suggested to be the most specific finding because the characteristic metaphyseal striations might not be apparent at young ages.[10] Multiple affected siblings with SPONASTRIME dysplasia have been reported,[1,2,6] and thus, an autosomal-recessive inheritance pattern has been suspected. However, no gene has been associated with this disorder.

To identify a genetic basis for SPONASTRIME dysplasia, we performed whole-exome sequencing and identified variants in *TONSL* (MIM: 604546) in individuals with this diagnosis and in individuals with other skeletal dysplasia phenotypes. We used studies in knockout mouse and zebrafish models and functional studies in subject-derived fibroblasts to demonstrate the essential nature of TONSL and to show that reduced TONSL function is associated with replication fork and chromosomal instability, which most likely contributes to the phenotypes observed in individuals with bi-allelic *TONSL* variants.

Material and Methods

Human Subjects and Sequencing Studies

Informed consent for all subjects (except subject P11) was obtained in accordance with research protocols that were approved by the institutional review board at Baylor College of Medicine (BCM), the National Institutes of Health (NIH), or at local institutions prior to testing. The sample for subject P11 was obtained from the Cell Line and DNA Biobank from Patients Affected by Genetic Diseases (Telethon Network of Genetic Biobanks), and consent was obtained as per the protocol for Biobank submission.[11] For subjects P2, P3-1, P4, P7-1, and P7-2, informed consent for publication of photographs was obtained.

DNA was extracted from peripheral blood mononuclear cells for exome sequencing. For families 1, 2, 9, and 11, exome sequencing was performed at the Human Genome Sequencing Center (HGSC) at BCM. We used 1 ug of DNA to construct an Illumina paired-end pre-capture library according to the manufacturer's protocol (Illumina Multiplexing_SamplePrep_Guide_1005361_D) and made modifications as described in the BCM-HGSC Illumina Barcoded Paired-End Capture Library Preparation protocol. Pre-capture libraries were pooled into 4-plex library pools and then hybridized in solution to the HGSC-designed core capture reagent[12] (52 Mb, NimbleGen) or pooled into 6-plex library pools with the custom VCRome 2.1 capture reagent1 (42 Mb, NimbleGen) according to the manufacturer's protocol (NimbleGen SeqCap EZ Exome Library SR User's Guide) with minor revisions. The sequencing run was performed in paired-end mode via the Illumina HiSeq 2000 platform; sequencing-by-synthesis reactions were extended for 101 cycles from each end, and an additional 7 cycles were performed for the index read. The sample had a sequencing yield of 10.6 Gb and 91% of the targeted exome bases were covered to a depth of 20× or greater. The Illumina sequence analysis was performed with the HGSC Mercury analysis pipeline,[13,14] which moves data through various analysis tools from the initial sequence generation on the instrument to annotated variant calls (SNPs and intra-read indels). For subject P3-1, trio exome sequencing was performed at Associated Regional and University Pathologists (ARUP) Laboratories with Illumina SureSelect XT kit reagents and a HiSeq2500 platform (Illumina), and the identified variants in *TONSL* were confirmed in subject P3-2 by Sanger sequencing. For family 5, exome capture was performed at the genomic platform of the IMAGINE Institute with the SureSelect Human All Exon kit (Agilent Technologies). Agilent SureSelect Human All Exon (V4) libraries were prepared from 3 μg of genomic DNA sheared with Ultrasonicator (Covaris), as recommended by the manufacturer. Barcoded exome libraries were pooled and sequenced with HiSep2500 (Illumina), generating paired-end reads. After demultiplexing, sequences were mapped on the human genome reference (NCBI build 37 [UCSC hg19] version) with Burrows-Wheeler Aligner (BWA).[15] The mean depth of coverage obtained for each sample was ≥80×, and 95% of the exome was covered at least 15×. Variant calling was carried out with the Genome Analysis Toolkit (GATK),[16] SAMtools,[17] and Picard Tools. Single-nucleotide variants (SNVs) were called with GATK Unified Genotyper, whereas indel calls were made with the GATK IndelGenotyper_v2. All variants with a read coverage ≤2× and a Phred-scaled quality of ≤20 were filtered out. All the variants were annotated and filtered with an in-house-developed annotation software system (Polyweb, unpublished data). We first focused our analyses on non-synonymous variants, splice variants, and coding indels. The potential

New York Presbyterian, New York, NY 10032, USA; [28]Clinical Genetics Unit, Instituto da Criança, Hospital das Clínicas da Faculdade de Medicina da Universidade de São Paulo, São Paulo, SP 05403-000, Brazil; [29]Centro de Pesquisa sobre o Genoma Humano e Células-Tronco, Instituto de Biociências da Universidade de São Paulo, SP 05508-0900, Brazil; [30]Departments of Psychiatry and Behavioral Sciences and Pediatrics, Kansas University Medical Center, Kansas City, KS 66160, USA; [31]Department of Ophthalmology and Vision Sciences, the Hospital for Sick Children, University of Toronto, Toronto, ON M5G 1X8, Canada; [32]Department of Allergy and Immunology, Sidra Medicine, Hamad Medical Corporation, Weill Cornell Medicine, Qatar, Doha, Qatar; [33]Department of Molecular, Cell, and Developmental Biology and Department of Orthopaedic Surgery, University of California, Los Angeles, Los Angeles, CA 90095, USA; [34]Department of Orthopaedic Surgery, Department of Human Genetics and Department of Obstetrics and Gynecology, David Geffen School of Medicine at UCLA, University of California, Los Angeles, Los Angeles, CA 90095, USA; [35]Medical Research Council Human Genetics Unit, Institute of Genetics and Molecular Medicine, University of Edinburgh, Edinburgh EH4 2XU, UK; [36]North East Thames Regional Genetics Service, Great Ormond Street Hospital, London WC1N 3JH, UK; [37]Department of Oncology and Metabolism, Academic Unit of Child Health, University of Sheffield, Sheffield S10 2TH, UK; [38]Department of Pediatrics, Division of Medical Genetics, University of Utah, Salt Lake City, UT 84112, USA
[39]These authors contributed equally to this work
[40]These authors contributed equally to this work
*Correspondence: blee@bcm.edu
https://doi.org/10.1016/j.ajhg.2019.01.007.

pathogenicity of variants was evaluated with the SIFT[18] (cutoff ≤ 0.05), PolyPhen2[19] (HumVar scores, cutoff ≥ 0.447), and Mutation Taster[20] (cutoff: qualitative prediction as pathogenic) prediction algorithms. We also assessed frequency in control populations and datasets, including the ExAC database, Single Nucleotide Polymorphism Database (dbSNP) 129, the 1000 Genomes project, ClinVar, HGMD, and in-house exome data. All variants (except the variants in subject P14) were confirmed by Sanger sequencing, and correct family segregation was verified. For family 6, exome sequencing was performed as described previously.[21] Family 7, which was enrolled in the Undiagnosed Diseases Network, and family 8 had exome sequencing performed at Baylor Genetics Laboratories, as described elsewhere.[22] Researchers used Codified Genomics (variation interpretation software) for variant review in families 7 and 8. Exome sequencing and analysis were performed as described previously for subject P10,[23] subject P12,[24] and subject P13.[24] For subject P14, the exome was sequenced at Centro de Pesquisa sobre o Genoma Humano e Células-Tronco (CEGH-CEL)-Universidade de São Paulo, the capture library was an Illumina TrueSeq kit, sequencing was done an on Illumina HiSeq, alignment was done with BWA, and annotation was done with GATK and ANNOVAR. Sanger sequencing of the *TONSL* exons was performed in DNA from subjects P4 and P15 with the primers in Table S1. Sanger confirmations were performed with the Big Dye Terminator v3.1 and an ABI 3730 DNA Analyzer (Life Technologies). Sanger confirmation for subject P2 was performed by submission of PCR products to Genewiz. All variant nomenclature uses hg19, GenBank: NM_013432.4.

Tonsl$^{-/-}$ Mouse Generation and Analysis

Single-guide RNAs (sgRNAs) were selected to target intronic sequences flanking exons 12–18 of *Tonsl* (chr15: 76,635,006–76,635,028 and chr15: 76,632,468–76,632,490; Genome Reference Consortium Mouse Build 38 (GRCm38) [mm10]) from the Wellcome Trust Sanger Institute (WTSI) Genome Editing website.[25] DNA templates for *in vitro* transcription of sgRNAs were produced through the use of overlapping oligonucleotides in a high-fidelity PCR reaction,[26] and sgRNA was transcribed with the MEGAshortscript T7 kit (Thermo Fisher). Cas9 mRNA was purchased from Thermo Fisher. Cas9 mRNA (100 ng/μl) and sgRNA (10 ng/μl) in RNase-free 1×PBS were injected into the cytoplasm of 100 pronuclear stage C57BL/6NJ embryos. We used primers P1 (5′-CTTCAG CTGGTGGCCACAT-3′), P2 (5′-TCTCCCATGTCATTGCGCC-3′), and P3 (5′-GCCCTCTCTAAGGCCCATAG-3′) for genotyping and sequencing the founder animals and subsequent generations (P1 and P2 amplify the wild-type (WT) allele; P1 and P3 amplify the null allele). All mouse studies were approved by the BCM institutional animal care and use committee (IACUC).

tonsl$^{-/-}$ Zebrafish Generation and Analysis

Zebrafish were raised according to standard protocols[27] and in accordance with University of Oregon IACUC protocols. We used Oregon AB* and *Tg(mpx:GFP)*^{i114} lines[28]. The zebrafish-codon-optimized Cas9 plasmid[29] that was digested with *Xba*I was purified and transcribed with the T3 message machine kit (Ambion). Guide RNA (gRNA) was designed (with the ZiFiT Targeter software) to the CRISPR target sequence 5′-GGAGAGTGCTA TGCAGAGCT-3′ at the 3′ end of *tonsl* exon 3. Templates for gRNA synthesis were prepared by PCR with the gene-specific primer 5′-AATTAATACGACTCACTATA-[20 bp target sequence]-GTTTTAG AGCTAGAAATAGC-3′ and the gRNA scaffold primer 5′-GATCCG CACCGACTCGGTGCCACTTTTTCAAGTTGATAACGGACTAGCC TTATTTTAACTTGCTATTTCTAGCTCTAAAAC-3′ at an annealing temperature of 60° C. sgRNA was synthesized with the T7 MEGAscript kit (Ambion). Cas9 mRNA (300 ng/μl) and sgRNA (150 ng/μl) were mixed and injected into Oregon AB* WT zebrafish embryos at the one-cell stage with an MPPI-2 Pressure Injector with a BP-15 Back Pressure Unit (Applied Scientific Instrumentation). We confirmed CRISPR activity at the target site with a sequence analysis of pools of injected embryos at 24 hours post-fertilization (hpf) by using primers Tonsl e3-6F 5′-CCCTAGGT GACTATCAAGCTGC-3′ and Tonsl e3+129R 5′-ACATGCATGC GTTTACTGTAGC-3′ to amplify the region containing the target sequence. Analysis of individual F1 embryos at 24 hpf identified clutches carrying frameshift mutations; the clutches were then propagated and crossed so the recessive phenotype could be examined. Two frameshift deletions of 5 and 13 bp, respectively, affecting both alternate 5′–3′ reading frames in exon 3, were recovered in the F1 progeny of injected founders. Skeletal elements were stained with Alcian blue and Alizarin red as previously described.[30] Images were captured with a Leica S8APO dissecting microscope fitted with a Leica EC3 camera and LAZ EZ imaging software. Statistical analyses were performed with GraphPad software.

Cell Culture and Generation of Cell Lines

Dermal primary fibroblasts were grown from skin-punch biopsies and maintained in Dulbecco's modified Eagle's medium (DMEM; Life Technologies) supplemented with 20% fetal calf serum (FCS), 5% L-glutamine, and 5% penicillin-streptomycin (Invitrogen) antibiotics. Subject-derived cell lines were validated by Sanger sequencing and immunoblotting. Primary fibroblasts were immortalized with 293FT-derived supernatant containing a human telomerase reverse transcriptase (TERT) lentivirus that was generated with the plasmids pLV-hTERT-IRES-hygro (gift from Tobias Meyer; Addgene #85140), psPax2 (gift from Didier Trono; Addgene #12260), and pMD2.G (gift from Didier Trono; Addgene #12259). Selection was performed with hygromycin (Invitrogen) at 70 μg/mL. Fibroblast complementation was carried out with a lentiviral vector that encoded Flag-tagged *TONSL* (gift from Dr. Yonghwan Kim). All cell lines were routinely tested for mycoplasma. ATLD2 is a fibroblast cell line derived from an individual who has both ataxia-telangiectasia-like disorder (ATLD, MIM: 604391) and bi-allelic, pathogenic variants in *MRE11* (MIM: 600814).[31]

Immunoblot Analysis and Antibodies

Whole-cell extracts were prepared from harvested subject-derived fibroblasts by sonication in UTB buffer (8 M urea, 50 mM Tris, 150 mM β-mercaptoethanol). Whole-cell extracts were then analyzed by sodium dodecyl sulfate polyacrylamide gel electrophoresis (SDS–PAGE) on 6% acrylamide gels according to standard procedures. Protein samples were transferred onto a nitrocellulose membrane, and immunoblotting was performed with antibodies to TONSL (1:200; the kind gift of D. Durocher)[32] and DNA-PK$_{CS}$ (Santa Cruz Biotechnology, [G-4] sc-5282; 1:2000).

Immunofluorescence and Fluorescence Microscopy

Subject-derived fibroblasts were seeded onto coverslips at least 48 h before extraction and fixation. Cells were pre-extracted for 5 min on ice with ice-cold buffer (25 mM HEPES [pH 7.4], 50 mM NaCl, 1 mM EDTA, 3 mM $MgCl^2$, 300 mM sucrose, and 0.5% Triton X-100) and then fixed with 4% paraformaldehyde

for 10 min. Fixed cells were stained with primary antibodies specific to γH2AX (Millipore, 05-636; 1:1,000) and RAD51 (Merck, PC130; 1:500), and with secondary antibodies conjugated to Alexa Fluor 488 and Alexa Fluor 594 (Life Technologies) and then stained with DAPI. Images were visualized with a Nikon Eclipse Ni microscope with NIS-Elements software (Nikon Instruments) and captured with a 100× oil-immersion objective lens.

DNA Fiber Spreading Assay

Subject-derived fibroblasts were seeded for at least 48 h prior to harvesting. Cells were pulse-labeled with 25 μM CldU for 30 min, washed with PBS, pulse-labeled with 250 μM IdU with or without 50 nM CPT, and harvested by trypsinization. The cells were washed with PBS and resuspended to a concentration of 5×10^5/mL in PBS. The cells were then lysed in spreading buffer (200 mM Tris-HCl [pH 7.5], 50 mM EDTA, 0.5% SDS) directly on glass microscope slides, and DNA fibers were allowed to spread down the slide by gravity. The slides were then fixed in methanol:-acetic acid (3:1 ratio) and denatured with 2.5 M HCl, and CldU and IdU were detected via rat anti-BrdU antibody (clone BU1/75, ICR1; Abcam, ab6326; 1:750) and mouse anti-BrdU antibody (clone B44; BD Biosciences, 347583; 1:750). The slides were fixed in 4% paraformaldehyde before being immunostained with secondary antibodies conjugated to Alexa Fluor 594 or Alexa Fluor 488 (Life Technologies). Labeled DNA fibers were visualized with a Nikon Eclipse Ni microscope with 60× oil-immersion objective lenses, and images were acquired with NIS-Elements software (Nikon Instruments). Replication fork structures (>1000 fork structures) and CldU and IdU track lengths (>300 ongoing forks) were then quantified with ImageJ software (US NIH).

Metaphase Spreads

Giemsa-stained metaphase spreads were prepared as previously described.[21] In brief, colcemid (KaryoMAX, Life Technologies) was added at a final concentration of 0.2 μg/mL for 4 h. The cells were then harvested by trypsinization, subjected to hypotonic shock for 30 min at 37° C in hypotonic buffer (10 mM KCl, 15% FCS), and fixed in 3:1 ethanol:acetic acid solution. The cells were dropped onto acetic-acid-humidified slides, stained for 15 min in Giemsa-modified solution (Sigma; 5% vol/vol in water), and washed in water for 5 min.

Statistics

Statistical analysis was performed as indicated in the tables and in the figure legends. A p value of less than 0.05 indicates significance.

Results

Bi-allelic *TONSL* Variants Cause a Spectrum of Skeletal Dysplasia Phenotypes

We performed exome sequencing in 10 probands with a clinical diagnosis of SPONASTRIME dysplasia; the probands were identified by the Baylor-Texas Children's Hospital Skeletal Dysplasia Program, the International Skeletal Dysplasia Registry, GeneMatcher,[33] and various collaborators who are experts in skeletal dysplasias (Tables 1, S2, and S3). Bi-allelic variants in *TONSL*, which encodes the Tonsoku-like DNA repair protein, were identified in six of the ten subjects with SPONASTRIME dysplasia (Table 2). Two additional subjects (subjects P4 and P15) with SPONASTRIME dysplasia and bi-allelic variants in *TONSL* were identified by Sanger sequencing of the coding region of the gene (Tables 1, 2, and S2). In addition, subject P3-2 was confirmed by Sanger sequencing to have the same variants in *TONSL* as his sibling (subject P3-1). These nine subjects had significant disproportionate short stature, spine abnormalities, and characteristic facial features, including midface hypoplasia with a depressed nasal bridge (Figures 1A and S1 and Table S2). All but the youngest subject (subject P3-2) also had metaphyseal striations. Other features included bilateral cataracts in three subjects, subglottic stenosis in three subjects, shallow dental roots in four subjects, and a history of hypogammaglobinemia in two subjects. Clinical information about subjects P4 and P15 has been published previously.[4,7,8] Bi-allelic variants in *TONSL* or in *MMS22L* (MIM: 615614), the gene encoding the binding partner for TONSL, were not detected in the other four subjects with a clinical diagnosis of SPONASTRIME dysplasia (subjects P9–12), suggesting that this phenotype is genetically heterogeneous (Table S3). However, single heterozygous variants in *TONSL* were identified in subjects P9 and P10 (the c.2800C>T [p.Arg934Trp] variant, which was also identified in individuals 1, 3, 14, and 15, and a variant predicted to impact splicing, respectively). Thus, we cannot rule out the possibility that deep intronic variants, promoter variants, large intragenic rearrangements, or large intragenic deletions in *TONSL* could be present in subjects P9–12. In the two subjects without any *TONSL* rare variants (subjects P11 and P12), exome analysis did not identify any sharing of genes with rare variants, nor did the analysis reveal any variants in genes encoding for TONSL interactors or related proteins.

Simultaneously, exome sequencing independently revealed bi-allelic variants in *TONSL* in three subjects (subjects P7-1, P7-2, and P8) (from two families) with spondylometaphyseal dysplasia and immunologic and hematologic abnormalities (hypogammaglobulinemia and neutropenia, respectively) and in subject P6, who had spondylometaphyseal dysplasia with severe short stature, primary aphakia, and absent pupils. Detailed clinical information is provided in Tables 1, 3, S2, S3, and S4 and Figures 1A and S1. All individuals except two (subjects P3-1 and P3-2) had a frameshift, nonsense, or splice variant in combination with a missense variant in *TONSL*. All missense variants had CADD scores greater than 15,[34] and all but one of the missense variants were predicted to be damaging or probably damaging by both SIFT and PolyPhen-2.[18,19] The variants are provided in Tables 2 and 4 and in Figure 1B. Details regarding the exome analysis are provided in Table S5.

Because all subjects except the siblings from family 3 had one frameshift, nonsense, or splice variant associated with an amino acid substitution, we hypothesized that bi-allelic partial loss of TONSL function might explain the phenotype in our subjects. To investigate the impact that the variants identified in our subjects had on TONSL protein stability, we performed immunoblot analyses on three subject-derived

Table 1. Skeletal Features of Subjects Diagnosed with SPONASTRIME Dysplasia

Subject ID	1	2	3-1	3-2	4	5	13	14	15
Sex	f	f	m	m	f	f	m	f	m
Age at Last Follow-up	7 years, 9 months	7 years, 11 months	4 years, 9 months	9 months	22 years	23 years	17 years, 10 months	4 years	11 years
Height (Z score)	−3.3	−4.2	−5.0	−9.0	−10.8	−8.8	−5.1	−6.7	−6.0
Weight (Z score)	−0.1	−1.2	−2.1	−5.1	−4.2	−3.0	−2.4	−2.2	−4.0
FOC (Z score)	N/A	N/A	−0.6	N/A	−3.4	−2.1	0.6	−1.0	−3.0
Disproportionately Short Stature	yes	yes	yes	yes	yes	yes	no	yes	yes
Orthopedic Abnormalities	none	genu valgum; leg length discrepancy; Perthes versus avascular necrosis[a]	rhizomelia; brachydactyly	rhizomelia; brachydactyly	rhizomelia and mesomelia; short, broad hands and feet	mildly short hands and feet	knee pain but no surgeries or joint dislocations	kyphoscoliosis; hyperlordosis; joint laxity; genu valgum	genu valgum (s/p surgery); leg length discrepancy; brachydactyly
Radiographic Features									
Metaphyses	widened metaphyses with striations and irregularities	metaphyseal irregularities	broad, flared with striations and irregularities	broad and flared	metaphyseal striations with irregularities	widened metaphyses with striations and irregularities	irregular, with striations	metaphyseal striations with irregularities	striations and irregularities, most notably in distal femurs and proximal tibias
Epiphyses	normal	unknown	small epiphyses which progressed to flattened epiphyses	normal	unknown	normal	normal	normal	small; delayed ossification
Spine	platyspondyly	platyspondyly	platyspondyly	platyspondyly	platyspondyly with biconcave vertebrae; progressive, severe double curve scoliosis	platyspondyly; biconcave vertebrae	biconcave vertebrae with mild platyspondyly	mild platyspondyly; some vertebral bodies with biconcave endplates	biconcave deformities; pear-shaped vertebral bodies; progressive decrease in interpedicular distances
Other Skeletal Findings	short, wide femoral necks	unknown	shallow acetabula with prominent ischial component; genu valgum	squaring of iliac wings	very short, irregular femoral necks; coxa vara; ivory epiphyses (hand); dislocated left hip with pseudoacetabulum	short femoral neck; coxa vara	exaggerated lumbar lordosis	none	slightly short and wide femoral necks

Abbreviations are as follows: f = female, m = male, FOC = frontal occipital circumference, and N/A = not available.
[a]Reported by parents after evaluation.

Table 2. Variants in *TONSL* in Subjects with a Clinical Diagnosis of SPONASTRIME Dysplasia

Family ID	1	2	3	4	5	13	14	15
Variant 1	c.2800C>T, (p.Arg934Trp)	c.1459G>A, (p.Glu487Lys)	c.2800C>T, (p.Arg934Trp)	c.1480G>A, (p.Glu494Lys)	c.1459G>A, (p.Glu487Lys)	c.3096dupA, (p.Gln1033Thrfs*57)	c.2800C>T, (p.Arg934Trp)	c.2800C>T, (p.Arg934Trp)
rsID	dbSNP: rs755575416	dbSNP: rs563710728	dbSNP: rs755575416	dbSNP: rs775551492	dbSNP: rs563710728	N/A	dbSNP: rs7555754	dbSNP: rs755575416
Frequency (gnomAD)	1/150710	21/239692	1/150710	1/30966	21/239692	not present	1/150710	1/150710
PolyPhen	probably damaging	probably damaging	probably damaging	benign	probably damaging	N/A	probably damaging	probably damaging
Sift	damaging	damaging	damaging	tolerated	damaging	N/A	damaging	damaging
CADD	16.77	21.3	16.77	16.12	21.3	N/A	16.77	16.77
Variant 2	c.460C>T, (p.Gln154*)	c.1602_1612del, (p.Ala536Glyfs*17)	c.3589T>C, (p.Ser1197Pro)	c.2638_2647delinsGG, (p.Arg880Glyfs*10)	c.1864dup, (p.Ala622Glyfs*67)	c.122-5C>G	c.3796dupA, (p.Arg1266Lysfs*23)	c.2407C>T, (p.Gln803*)
rsID	dbSNP: rs1026265047	N/A	N/A	N/A	dbSNP: rs762903420	N/A	dbSNP: rs782733226	dbSNP: rs769100855
Frequency (gnomAD)	2/243938	not present	not present	not present	not present	not present	2/251402	2/219724
PolyPhen	N/A	N/A	probably damaging	N/A	N/A	N/A	N/A	N/A
Sift	N/A	N/A	damaging	N/A	N/A	N/A	N/A	N/A
CADD	N/A	N/A	15.56	N/A	N/A	N/A	N/A	N/A

All coordinates utilize hg19 (GenBank: NM_013432.4). Parental DNA for subjects P13 and P15 was not available to ascertain segregation. Variant c.122-5C>G was assessed with dbscSNV[55] and Human Splicing Finder 3.1,[56] but the effects did not reach statistical significance. Abbreviations are as follows: N/A = not available.

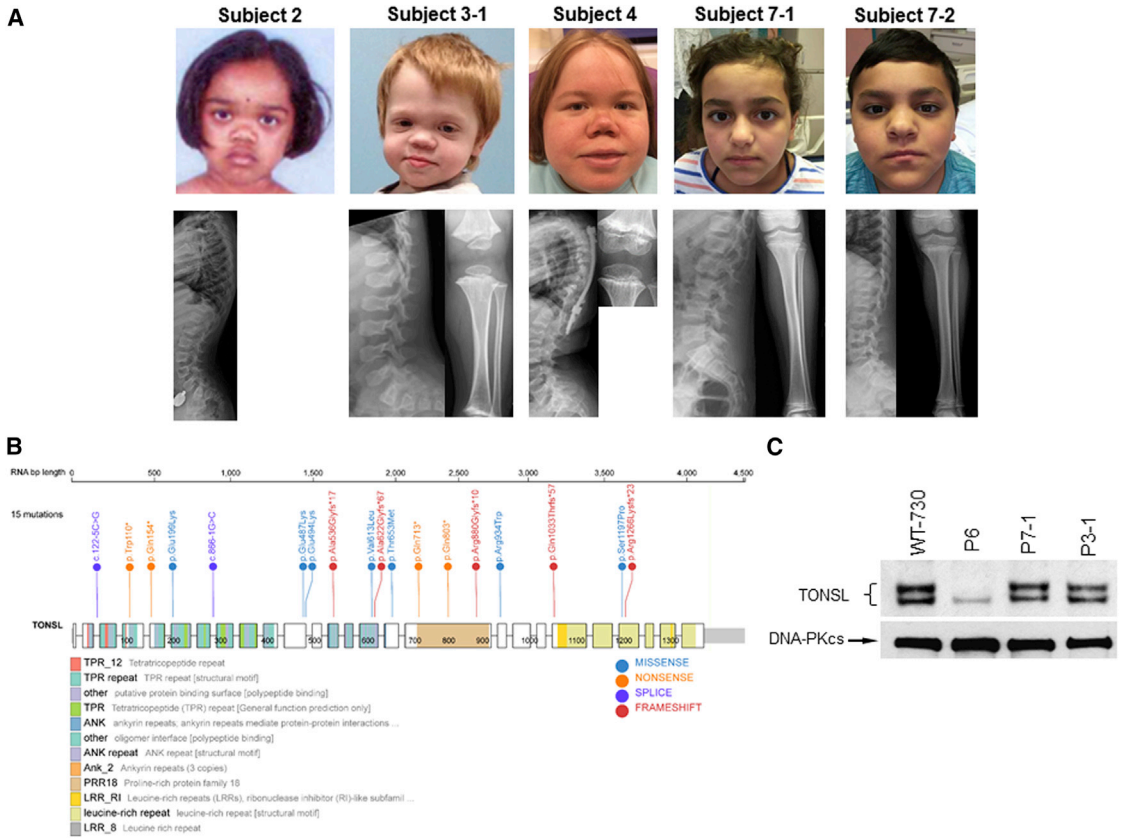

Figure 1. *TONSL* Variants in Subjects with Skeletal Dysplasias

(A) Subject photographs and radiographs. The characteristic facial features of SPONASTRIME dysplasia (midface hypoplasia and a depressed nasal root) are more evident in subjects P2, P3-1, and P4. Characteristic features of the spine are demonstrated through biconcave vertebrae in subjects P4, P7-1, and P7-2, and platyspondyly is demonstrated by subjects P2, P3-1, and P4. Metaphyseal striations are most evident in subjects P3-1 and P4.

(B) Pathogenic variants identified in subjects with various skeletal dysplasias.

(C) Immunoblot demonstrating reduced protein in subject P6 but apparently normal protein levels in subjects P7-1 and P3-1. DNA-PKcs was used as a loading control. The X-ray showing the metaphyseal striations in subject P4 is reproduced from Offiah et al.[8] with permission from BMJ Publishing Group.

fibroblast cell lines that had a range of *TONSL* variants. This analysis revealed that the cell line from subject P6 (c.2137C>T, [p.Gln713*]; c.1958C>T, [p.Thr653Met]) produced little to undetectable levels of full-length TONSL protein (Figure 1C), perhaps reflecting the deleterious impact of the two variants on TONSL protein stability. However, because the antibody we used was raised against a recombinant-TONSL fragment comprising residues 559–809, a region encompassing both mutations in subject P6, it cannot be ruled out that the absence of a signal might result from the loss of the epitope recognition. Interestingly, in contrast, near-normal levels of TONSL protein were detected in cell lines derived from subjects P3-1 (c.2800C>T [p.Arg934Trp]; c.3589T>C [p.Ser1197Pro]) and P7-1 (c.866−1G>C; c.595G>A [p.Glu199Lys]) (Figure 1C), indicating that individual *TONSL* variants have a differential effect on protein stability. Of note, the anti-TONSL antibody we used for immunoblotting detected two major bands. Although the origin of these is unclear, we hypothesize that they represent either different isoforms or that this is caused by post-translational modification of the protein.

Early Lethality in Mouse and Zebrafish Models of TONSL Deficiency

To investigate the impact of TONSL deficiency on development with *in vivo* models, we identified a *Tonsl* knockout mouse that was generated by the BCM Knockout Mouse Phenotyping Program (KOMP2). Exons 12 to 18 of *Tonsl* were deleted in a knockout mouse (*Tonsl*$^{em1(IMPC)Bay}$, *Tonsl*$^{-/-}$) that was generated via CRISPR-Cas9 technology as described previously (Figure S3).[35,36] Deletion of these exons is predicted to result in a frameshift and a premature stop codon, leading to nonsense mediated decay. In collaboration with KOMP2, we detected no homozygous *Tonsl*$^{-/-}$ mice at weaning (Table 5). Moreover, we performed embryonic genotyping, and we detected no homozygous mice as early as E9.5, suggesting that murine *Tonsl* deficiency causes lethality early in embryogenesis (Table 5).

To further investigate the impact of TONSL deficiency on embryonic development, we used CRISPR-Cas9 to generate early frameshift mutations in the zebrafish *tonsl* gene (Figure S4). Zebrafish *tonsl*$^{-/-}$ mutants undergo normal embryonic development and are indistinguishable

Table 3. Skeletal Features for Subjects without a Clinical Diagnosis of SPONASTRIME Dysplasia

Subject ID	6	7-1	7-2	8
Diagnosis	spondylometaphyseal dysplasia	spondylometaphyseal dysplasia	spondylometaphyseal dysplasia	spondylometaphyseal dysplasia
Sex	f	f	m	f
Age at Last Follow-up	12 years	10 years, 9 months	9 years, 9 months	5 years, 11 months
Height (Z score)	−10.6	−1.5	−1.6	−6.5
Weight (Z score)	−5.1	−0.2	0.8	−5.3
FOC (Z score)	−8.0	0.1	−1.0	−4.3
Disproportionately Short Stature	no	no	no	yes
Orthopedic Abnormalities	long, tapering fingers and proximally inserted thumbs; long and overlapping toes	pes planus	none	rhizomelia and mesomelia; 5th finger clinodactyly
Radiographic Features				
Metaphyses	irregular	mild metaphyseal irregularities with mild striations	mild widening and irregularities with mild striations	broad, flared, and irregular metaphyses with mild striations
Epiphyses	normal	normal	normal	normal
Spine	platyspondyly	biconcave vertebrae	biconcave vertebrae	platyspondyly
Other Skeletal Findings	none	short, wide femoral necks	short, wide femoral necks	squaring of iliac wings; coxa valga

Abbreviations are as follows: f = female, m = male, and FOC = frontal occipital circumference.

from WT siblings up to 6 days post-fertilization (dpf), but they begin to show reduced fitness and delayed growth thereafter (Figures 2A and 2B); 100% mortality was observed before 20 dpf. Using cartilage and bone staining to examine skeletal development, we observed that ossification of vertebral bodies around the notochord was significantly accelerated in *tonsl*$^{-/-}$ larvae compared to WT siblings at 7 dpf (Figure 2C). Because of the clinical findings of neutropenia in a subset of individuals in this study, we crossed carriers of the truncating *tonsl* alleles into a transgenic zebrafish line in which neutrophils fluoresce from day 2 onward. We observed normal neutrophil development in *Tg(mpo:gfp;tonsl*$^{-/-}$*)* mutants through 6 dpf, after which diminishing neutrophil numbers correlated with the progressive fitness decline characteristic of these mutants (Figures 2D and 2E). Although analysis is somewhat limited by early lethality, the larval phenotypes are reminiscent of the short stature and immunologic and spinal abnormalities exhibited by individuals with pathogenic variants in *TONSL*; these characteristics get progressively worse with age and development (Tables 1, 3, S2, and S4). Together, these *in vivo* models of TONSL deficiency demonstrate the essential function of the protein.

Defective Formation of RAD51-Induced Foci in Fibroblast Cell Lines Derived from Individuals with *TONSL* Variants

TONSL is homologous to the plant DNA repair protein Tonsoku/Brushy1/Mgoun3 and, in conjunction with its obligate binding partner, MMS22L, is necessary for the repair of replication-associated DNA damage.[32,37–39] Although the TONSL-MMS22L complex is reported to bind to all replication forks, increased binding has been noted at stalled forks and DNA-damage sites,[32,37–40] where the complex promotes efficient homologous recombination (HR)-dependent repair and the restart of stalled replication forks by stimulating RAD51-ssDNA (single-stranded DNA) nucleofilament formation.[38,40] As a consequence, loss of TONSL leads to increased levels of S-phase-associated DNA damage and defective HR, and it renders cells hypersensitive to agents, such as the topoisomerase 1 inhibitor camptothecin (CPT), that induce DNA damage.[32,37–40]

Given the lethality of TONSL deficiency in murine and zebrafish models, we investigated the functional effects of *TONSL* variants in subject-derived cell lines. Fibroblast cell lines were successfully generated from three subjects and attempted in two additional subjects, but the cell lines from these two subjects failed repeatedly because of poor growth, a finding that was not unexpected given the function of TONSL during DNA replication. Consistent with the role of TONSL in promoting RAD51 nucleofilament formation, all three subject-derived cell lines exhibited defective formation of CPT-induced RAD51 foci as measured by immunofluorescence (Figures 3A and 3B).

After this, we used the DNA fiber technique to assess the impact of the *TONSL* variants on replication-fork dynamics.[41,42] This analysis revealed that all three subject-derived cell lines exhibited a significant increase in spontaneously stalled replication forks, along with a concurrent decrease in ongoing forks, demonstrating that defects in

Table 4. Variants in *TONSL* in Subjects without a Clinical Diagnosis of SPONASTRIME Dysplasia

Family ID	6	7	8
Variant 1	c.2137C>T, (p.Gln713*)	c.866−1G>C	c.329G>A, (p.Trp110*)
rsID	N/A	N/A	N/A
Frequency (gnomAD)	not present	not present	not present
PolyPhen	N/A	N/A	N/A
Sift	N/A	N/A	N/A
CADD	N/A	11.62	N/A
Variant 2	c.1958C>T, (p.Thr653Met)	c.595G>A, (p.Glu199Lys)	c.1837G>T, (p.Val613Leu)
rsID	dbSNP: rs755055463	N/A	N/A
Frequency (gnomAD)	4/244636	not present	not present
PolyPhen	probably damaging	probably damaging	probably damaging
Sift	damaging	damaging	damaging
CADD	20.8	36	21.5

All coordinates utilize hg19, GenBank: NM_013432.4. Variant c.866−1G>C is predicted to affect splicing by dbscSNV[55] and Human Splicing Finder 3.1.[56] Abbreviations are as follows: N/A = not available.

TONSL give rise to replication fork instability (Figures 4A and 4B). We next investigated the ability of subject-derived cell lines to replicate in the presence of CPT. To this end, we performed DNA fiber analysis with a low dose of CPT (50 nM) co-incubated with the second label (IdU) (Figure 4A). We then measured IdU tract length (normalized to CldU tract length) as a readout of the rate of replication fork progression in the presence of CPT. Strikingly, two of the three subject-derived cell lines (P6 and P7-1) exhibited significantly reduced rates of replication fork progression in the presence of CPT (expressed as a ratio of IdU/CldU tract length) (Figure 4C); this is consistent with the role of TONSL in promoting DNA replication in the presence of DNA damage.[37] The P3-1 cell line did not exhibit a detectable reduction in replication fork progression upon CPT exposure. This raises the possibility either that not all of the *TONSL* variants have the same level of impact on TONSL function or that the DNA fiber assay we used is not sensitive enough to detect mild defects in replication fork progression. However, these findings could, in part, explain the variation in clinical phenotypes exhibited by the individuals with *TONSL* variants.

To confirm that the observed cellular defects were due to variants in *TONSL*, we complemented two subject-derived fibroblast cell lines (P3-1 and P6) with either an empty vector or a vector expressing Flag-tagged WT *TONSL* via a lentiviral expression system (Figure 5A). Importantly, re-expression of WT *TONSL* rescued CPT-induced RAD51-foci formation and reduced the spontaneous replication fork instability observed in both P3-1 and P6 fibroblast cells lines (Figures 5B–5D). Furthermore, the reduced rate of replication fork progression exhibited by P6 in the presence of CPT was also corrected (Figure 5E).

Lastly, to ascertain the pathogenic impact that the increased replication fork stalling might have on genome stability, we assessed metaphase spreads from the complemented subject-derived fibroblast cell lines for increased spontaneous chromosome breakage. In keeping with the observed replication abnormalities, both subject-derived fibroblast cell lines complemented with the empty vector exhibited increased amounts of spontaneous chromosomal aberrations, which were rescued upon re-expression of WT *TONSL*. This demonstrates that the replication defects observed in subject-derived cell lines give rise to increased genome instability (Figures 6A and 6B). Taken together, these data confirm at the cellular level the pathogenicity of the *TONSL* variants identified in these cell lines derived from individuals with both the SPONASTRIME and non-SPONASTRIME dysplasia phenotypes.

Discussion

In this study, we demonstrate that bi-allelic *TONSL* variants are associated with a spectrum of skeletal dysplasia phenotypes, ranging from clinical SPONASTRIME dysplasia with marked disproportionate short stature to mild short stature with immunologic and hematologic abnormalities,

Table 5. Early Embryonic Lethality in *Tonsl*$^{-/-}$ Mice

Phenotype	Postnatal Day 14	Embryonic Day 9.5
Tonsl$^{+/+}$	59	7
Tonsl$^{+/-}$	125	26
Tonsl$^{-/-}$	0	0
Chi square, df	52.63, 2	10.43, 2
p value	< 0.0001	0.0054

Abbreviations are as follows: df = degrees of freedom.

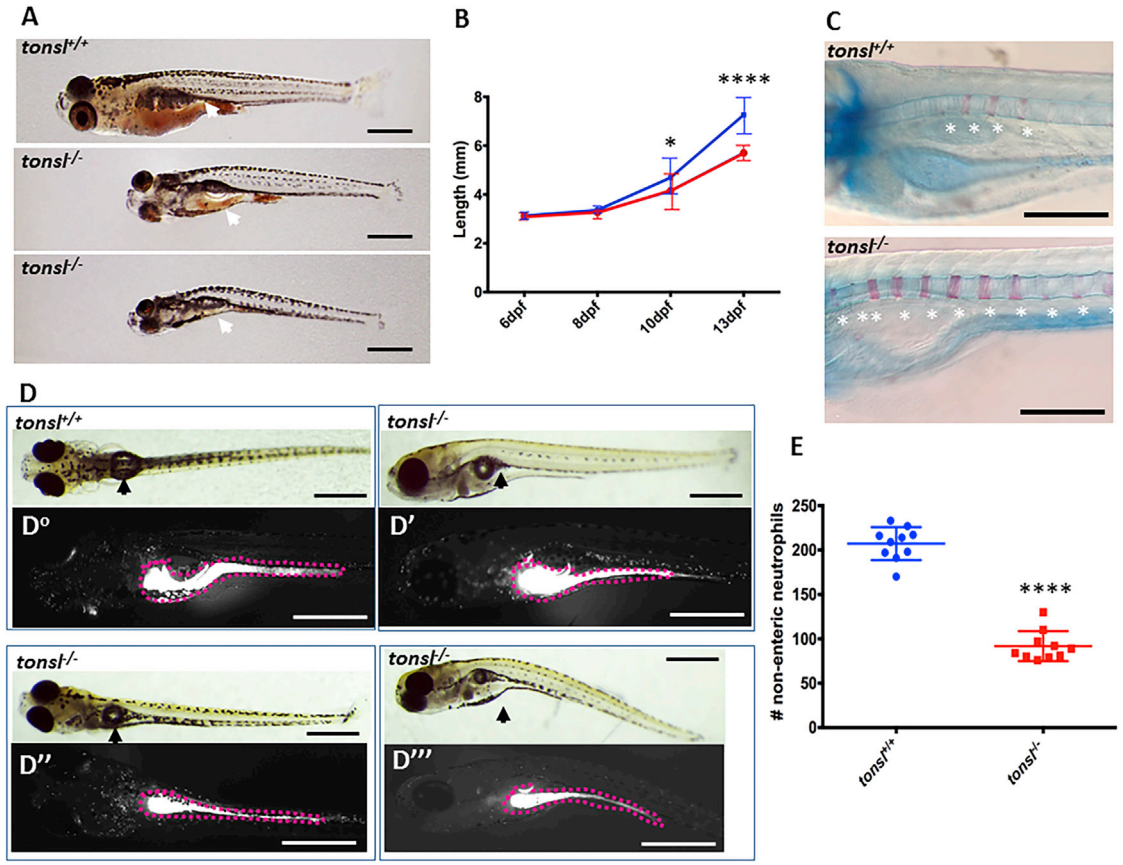

Figure 2. ***tonsl*$^{-/-}$ Zebrafish Are Larval Lethal and Have Growth Deficits, Vertebral Abnormalities, and Reduced Neutrophil Numbers**
(A) *tonsl*$^{-/-}$ zebrafish are larval lethal and show progressively diminished size compared to that of wild-type (WT) siblings. Food intake is variable in mutants, and reduced food intake correlates with reduced fitness and increased mortality (the gut contents of larvae at 13 dpf are indicated with white arrows).
(B) *tonsl*$^{-/-}$ fish (red) are not significantly smaller than WT siblings (blue) at 6 days post fertilization (dpf) or 8 dpf, but they are, on average, smaller at later time points through 13 dpf ($N \geq 10$ larvae for each time point; $p = 0.045$ at 10 dpf; $p < 0.0001$ at 13 dpf). Normal zebrafish growth during this stage varies widely, and survivor bias is a factor in these data because *tonsl*$^{-/-}$ mutants begin to die at 8 dpf.
(C) *tonsl* mutants exhibit precocious ossification of the axial skeleton. Bone formation is stained by Alizarin red, and cartilage is stained with Alcian blue. At 7 dpf, vertebral development is marked by bony centra forming around the notochord (asterisks). Significantly more centra have formed by this stage in homozygous *tonsl* mutants compared to WT siblings. WT—4.100 ± 0.5667, n = 10 larvae; *tonsl*$^{-/-}$:—8.867 ± 0.4350, n = 15 larvae.
(D) WT larvae have a high concentration of neutrophils in the gut (dashed outline), and neutrophils are dispersed throughout the circulatory system (D^{o}). *mpo:gfp;tonsl*$^{-/-}$ mutants have variable neutrophil distribution that is correlated with their decline in health; the distribution ranges from normal (D′) to reduced neutrophil fluorescence in the gut (D″ and D‴), and from normal to diminished numbers of circulating neutrophils observable in blood vessels of the head and trunk (D‴).
(E) Compared to stage-matched WT zebrafish (blue) *mpo:gfp;tonsl*$^{-/-}$, mutants showing signs of decline (D‴, red) had a reduced number of circulating neutrophils. Gut neutrophils were excluded from this count (n = 10; $p < 0.0001$). Scale bars in A and D = 1 mm; in C = 500 nm. Student's t tests with Welch's correlation were performed for each dataset. Data in (B) are mean ± SD. Error bars indicate standard deviation.

in 13 subjects from 11 families. We also show that several clinical features of these subjects are recapitulated by the zebrafish *tonsl* knockout model. Importantly, *TONSL* is the first gene to be associated with the SPONASTRIME dysplasia phenotype. However, we were unable to identify variants in *TONSL* or *MMS22L* in four subjects with a clinical diagnosis of SPONASTRIME dysplasia via exome sequencing. This result suggests that SPONASTRIME dysplasia is genetically heterogeneous. An alternative hypothesis is that noncoding variants in *TONSL* could contribute to the phenotype in these subjects; further genome-sequencing studies are warranted to rule out this possibility.

One striking finding from our study is the clinical variability of disease presentation and severity caused by pathogenic variants in the same gene. Although the majority of subjects with *TONSL* variants were clinically diagnosed with SPONASTRIME dysplasia or a disorder exhibiting many features consistent with SPONASTRIME dysplasia (subjects P6, P7-1, P7-2, and P8), a lack of diagnostic features (such as absent metaphyseal striations [subject P6] or short stature [subjects P7-1 and P7-2]) or the presence of atypical clinical abnormalities (such as severe microcephaly and primary aphakia [subject P6]; and congenital neutropenia [subjects P7-1, P7-2, and P8]) were noted in

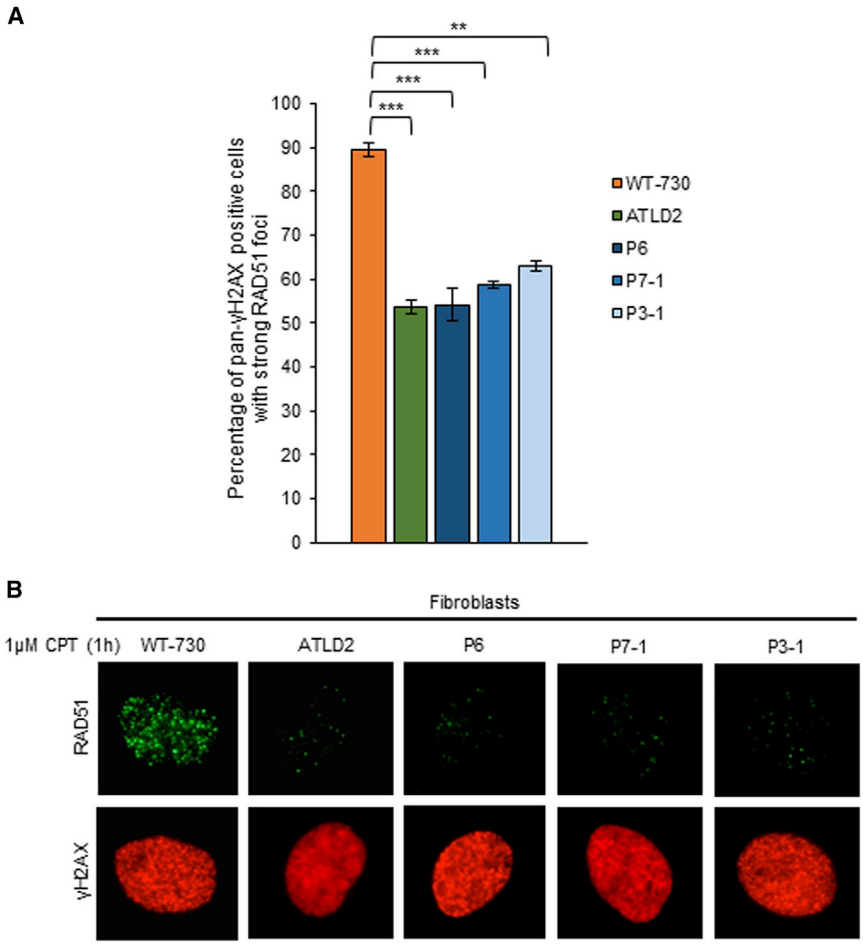

Figure 3. Impact of *TONSL* Variants on CPT-Induced RAD51 Foci Formation

(A) Cell lines derived from individuals with bi-allelic *TONSL* variants; the cell lines exhibit defective formation of RAD51 foci after CPT-induced DNA damage. RAD51-foci formation was analyzed by immunofluorescence in subject-derived fibroblasts exposed to 1 μM CPT; cells were stained with pan-nuclear γH2AX, and the percentage of those that exhibited "strong" RAD51 foci was quantified. ATLD2 is a fibroblast cell line derived from an individual with a confirmed genetic diagnosis of ataxia telangiectasia-like disorder (pathogenic variants in *MRE11*) and was used as a control. n = 3 independent experiments. A minimum of 400 cells was counted per experiment. A Student's t-test was performed for statistical analysis (** = $p < 0.01$ and *** = $p < 0.001$). Data in (A) show mean values, and error bars denote SEM; representative images are shown in (B).

some subjects. Interestingly, this phenotypic variability has also been noted in other skeletal dysplasias caused by pathogenic variants in replication/repair genes, such as *RECQL4* (MIM: 603780) and *SMARCAL1* (MIM: 606622).[43,44] Although the underlying cause of this clinical heterogeneity is unclear, it is most likely due, at least in part, to both the severity of the individual hypomorphic variants and the impact that each hypomorphic variant has on protein stability and/or function. Notably, several of the missense variants identified in the affected individuals localize within TONSL's central portion, which contains the ankyrin repeats; this portion of the protein was previously shown to be required to mediate its interaction with replisome components, its accumulation at damaged forks or DNA lesions, and its histone-chaperone and epigenetic-reader activity.[32,37,38] Furthermore, previous cell studies have demonstrated that deletions involving the ankyrin repeats lead to defective recruitment of TONSL to damaged replication fork sites and increased amounts of replication-associated DNA damage.[32,37,38] This finding suggests that the abnormal growth exhibited by individuals with *TONSL* variants might result from defective cellular replication beginning during development *in utero*. Consistent with this hypothesis, most subjects with bi-allelic variants in *TONSL* in our cohort presented with evidence of early short stature with reduced length in the newborn period. Moreover, all of the cell lines derived from affected individuals exhibited a significant increase in spontaneous replication fork stalling; this phenotype is commonly observed in cell lines derived from individuals with replication-defective-associated microcephalic dwarfism (MD), such as MD-DONSON (MIM: 617604), or microcephalic primordial dwarfism (MPD), such as ATR-Seckel syndrome (MIM: 210600) and MPD-TRAIP (MIM: 605958).[21,45] However, unlike in MD, individuals with variants in *TONSL* do not have microcephaly and have even lower Z scores for height at older ages than in the newborn period, suggesting that cell division in growth plate chondrocytes might be more severely impacted in this disorder.

In addition to having a role in promoting normal replication, TONSL also functions to repair and restart damaged replication forks through its ability both to chaperone histones[46,47] and to facilitate RAD51 loading.[40] Consequently, transient depletion of TONSL compromises a cell's capacity to replicate through DNA damage, particularly damage induced by the TOP1 inhibitor, CPT. All three of the subject-derived cell lines exhibited increased spontaneous replication fork stalling and defective formation of CPT-induced RAD51 foci, both of which could be rescued by the re-expression of WT *TONSL*. Interestingly, only two out of the three subject-derived cell lines tested exhibited a decreased ability to replicate through CPT-damaged DNA (P6 and P7-1). In contrast, despite exhibiting increased spontaneous replication fork stalling and defective formation of CPT-induced RAD51 foci, the cell line derived from subject P3-1 was able to efficiently replicate in the presence of CPT. Although unexpected, because

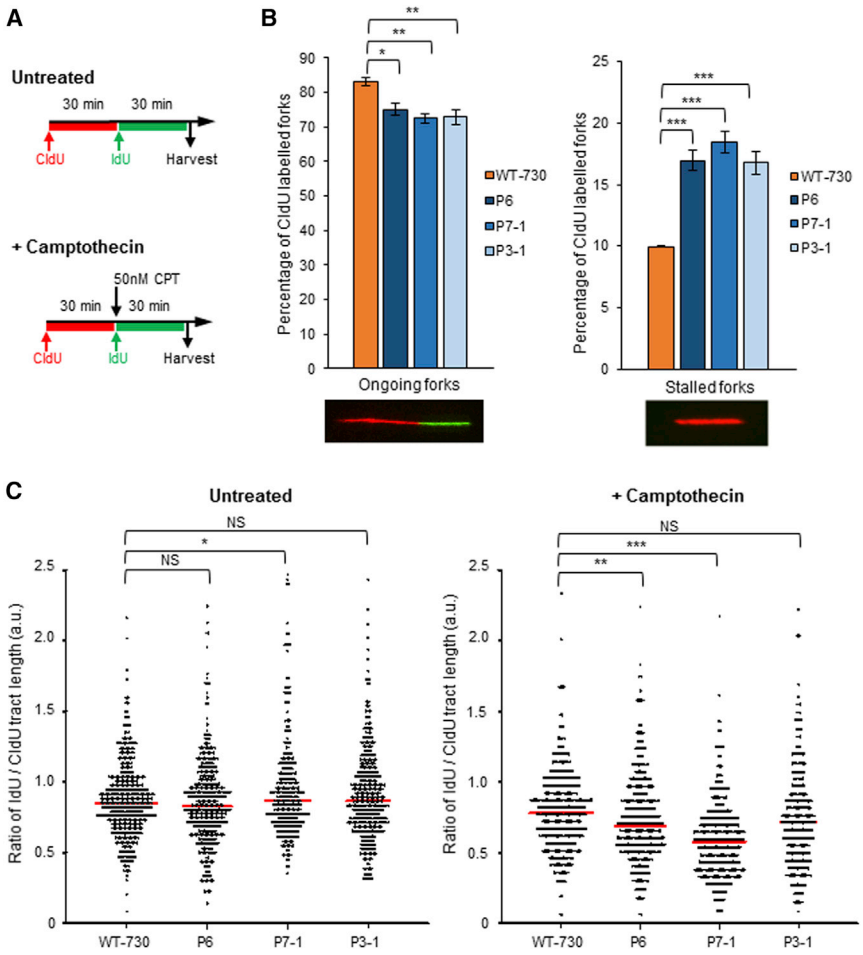

Figure 4. Cell Lines from Individuals with Bi-allelic *TONSL* Variants Exhibit Increased Levels of Spontaneous Replication Fork Stalling and Defective Replication Fork Progression in the Presence of CPT

(A) Schematic representation for DNA fiber analysis in the absence or presence of exogenous replication stress. Subject-derived cell lines were pulsed with CldU for 30 min, and then pulsed with IdU, or IdU with 50 nM CPT for 30 min.

(B) DNA fiber analysis of subject-derived fibroblast cell lines. The percentage of ongoing forks (left) or stalled forks (right) in the absence of exogenous DNA damage was quantified. Representative images of ongoing forks and stalled forks are included below. A minimum of 850 fork structures in total was counted over three independent experiments. A Student's t-test was performed for statistical analysis. Error bars denote SEM.

(C) Dot-density graph representation of the ratio of IdU tract length to CldU tract length in untreated and CPT-treated patient-derived fibroblasts. n = 3 independent experiments. A minimum of 100 ongoing fork structures was counted per experiment. Red lines denote mean values. A Mann-Whitney rank sum test was performed for statistical analysis. In all cases, * = $p < 0.05$, ** = $p < 0.01$, and *** = $p < 0.001$.

TONSL has been demonstrated to be required for both processes, it is possible that the variants in P3-1 are "separation-of-function" variants that disrupt the formation of RAD51 nucleofilaments at one-ended double strand breaks (DSBs) that are formed upon the CPT-induced collapse of replication forks, but the variants still promote replication in the presence of CPT via other mechanisms. Indeed, it has been suggested that RAD51 and its associated factors have both HR-dependent and -independent roles in promoting DNA replication and repair. For example, expression of a dominant negative RAD51 mutant (T131P) does not impact the ability of the cells to perform HR, but it renders cells unable to efficiently repair DNA interstrand cross-links.[48] Furthermore, pathogenic variants of the C-terminal RAD51-binding region of BRCA2 specifically compromise its role in protecting replication forks from uncontrolled nucleolytic processing, but the region still retains its ability to promote efficient HR-mediated repair of DSBs.[49] Therefore, this indicates that an inability of subject-derived cells to form RAD51 foci upon DNA damage is not necessarily indicative of a defect in all RAD51-dependent replication- and repair-associated functions and that these cellular processes should be tested specifically so that the pathway in which the cellular defect lies can be ascertained.

In addition to its role in dealing with replication-associated DNA damage, TONSL was recently implicated in repairing DNA DSBs.[50] DSBs are predominantly repaired by non-homologous DNA end joining (NHEJ) in the G1 and G2 phases of the cell cycle, but they can also be repaired by HR in the late S and G2 phases. Despite being structurally and biochemically distinct, the mechanisms underlying the HR-dependent repair of DSBs and stalled or damaged replication forks share substantial overlap. In a manner similar to the complex's response to replication-associated DNA damage, TONSL-MMS22L has been proposed to be recruited to newly deposited histones at DSB-end-resection sites, where it functions to promote HR by facilitating the loading of RAD51.[50] On the basis of this hypothesis, it is tempting to speculate that the more severely affected individuals with *TONSL* variants might have defects in the repair pathways for both replication damage and DNA DSBs, whereas those with a milder clinical phenotype only have deficiencies in one of the TONSL-dependent repair pathways.

It is not currently clear why the *TONSL* variants specifically give rise to skeletal abnormalities. Although skeletal abnormalities, especially short stature or dwarfism, are actually relatively common in human syndromes that are caused by pathogenic variants in replication fork stability factors or in the proteins involved in responding to replication-blocking lesions, the additional skeletal

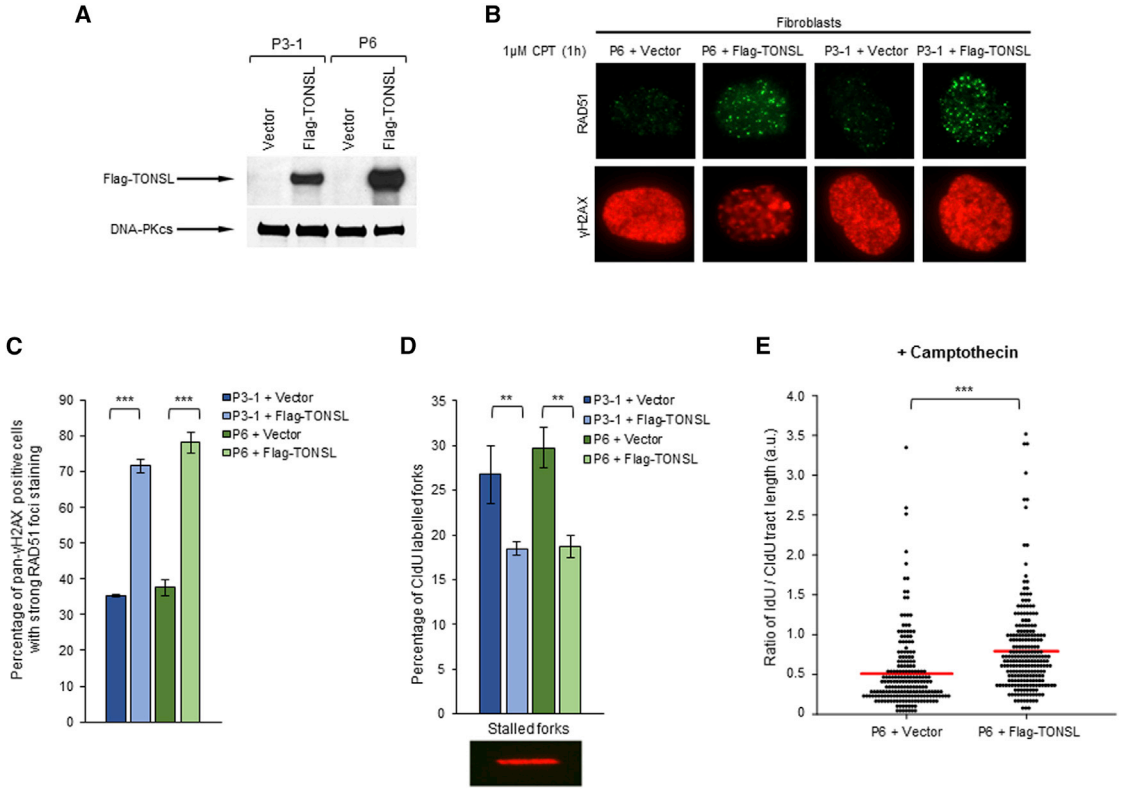

Figure 5. Wild-Type TONSL Rescues CPT-Induced RAD51 Foci Formation and Corrects the Replication Abnormalities Observed in Subject-Derived Fibroblasts

(A) Representative immunoblot analysis of TONSL in fibroblasts that were derived from subjects P3-1 and P6 and infected with lentiviruses that encoded either WT Flag-tagged TONSL or an empty vector. DNA-PKcs was used as a loading control.

(B and C) Fibroblasts cell lines from (A) were exposed to 1 μM CPT, and the percentage of cells with RAD51-foci formation was quantified as in Figure 3A. A minimum of 1,000 cells in total was counted over three independent experiments. A Student's t-test was performed for statistical analysis. Error bars denote SEM. Representative images are shown in (B).

(D) DNA fiber analysis was performed on subject-derived fibroblasts cell lines expressing either Flag-tagged WT TONSL or an empty lentiviral vector. The percentage of stalled forks in untreated cells was quantified. A minimum of 350 fork structures in total was counted over three independent experiments. A Student's T-Test was performed for statistical analysis. Error bars denote SEM.

(E) Dot-density graph representation of the ratio of IdU tract length to CldU tract length in CPT-treated fibroblasts. A minimum of 200 fork structures in total was counted over three independent experiments. A Mann-Whitney rank sum test was performed for statistical analysis. Red lines denote mean values. In all cases, *** = $p < 0.001$ and ** = $p < 0.01$.

features differ considerably depending on the specific gene that is mutated. For example, a diagnostic clinical feature of Schimke immunoosseous dysplasia (SIOD) (MIM: 242900) is spondyloepiphyseal dysplasia. In contrast, Fanconi anemia (MIM: 227650) is commonly, but not invariably, associated with radial ray abnormalities and vertebral anomalies. Thus, although normal replication and DNA repair are essential for bone development and growth, a defect in either of these processes does not necessarily give rise to the same specific skeletal abnormalities. Interestingly, however, the skeletal dysplasia phenotype associated with *TONSL* variants, and the variability of the clinical phenotype, seem to have more features in common with SIOD, which is caused by pathogenic variants in the DNA annealing helicase *SMARCAL1* (MIM: 606622), than with other replication disorders.[43,51] Although there have been no reports of SMARCAL1 interacting with or regulating RAD51 directly, it has been shown to promote the reversal of stalled or damaged replication forks; this reversal is a prerequisite for RAD51-dependent fork stabilization. As a result, it is tempting to speculate that the similarities in skeletal abnormalities exhibited by individuals with *TONSL* and *SMARCAL1* variants are linked to their ability to promote or stabilize reversed replication forks. However, why skeletal development would be particularly affected by loss of this function, which presumably would be essential for many cell types during development, is not known, especially since the expression of *TONSL* appears to be fairly ubiquitous.[52] Only the development of more clinically relevant animal models will be able to answer this question.

Another interesting aspect of the clinical phenotype exhibited by individuals with *TONSL* variants is the immunologic and hematological abnormalities. Although hypogammaglobulinemia is often observed in individuals with variants in genes that are involved in promoting DSB repair (such genes include *NBN* [MIM:602667], *ATM* [MIM:607585], *LIG4* [MIM:601837], *DCLRE1C*

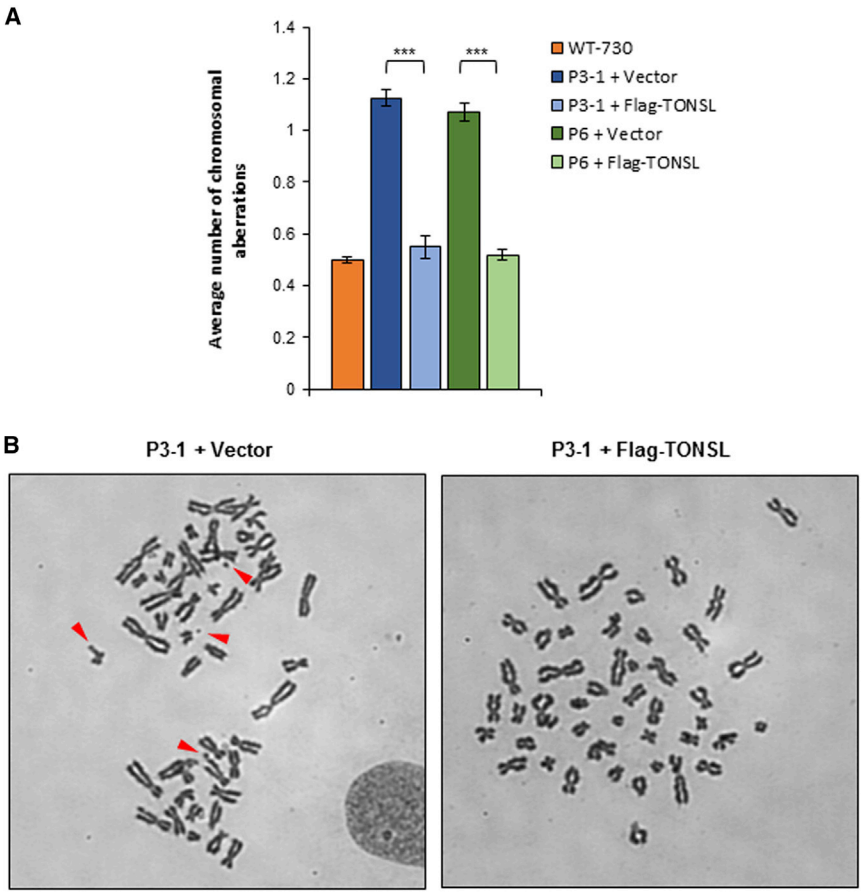

Figure 6. Subject-Derived Fibroblasts Exhibit Increased Levels of Spontaneous Chromosomal Aberrations

(A) Metaphase spreads were prepared from subject-derived fibroblast cell lines expressing either Flag-tagged WT TONSL or an empty lentiviral vector. The average number of spontaneous chromosomal aberrations per metaphase was quantified. n = 3 independent experiments. A minimum of 32 metaphases was counted for each experiment. A Student's t-test was performed for statistical analysis (*** = $p < 0.001$). Error bars denote SEM. Representative images of metaphase spreads are shown in (B).

[MIM:605988], or *NHEJ1* [MIM:611290]), it is not commonly associated with replication-deficiency disorders or defects in the HR pathway.[53] This suggests that perhaps TONSL plays an additional role in facilitating the repair of specialized DSBs, particularly those associated with immune-cell maturation and immunoglobulin gene rearrangement. In addition, several subjects exhibited neutropenia. Although this phenotype is relatively rare among both DNA repair and replication disorders, it has been documented in individuals with the hypomorphic variants *GINS1* (MIM: 610608) and *SMARCAL1*.[54] Currently it is not clear why the neutrophil lineage is specifically sensitive to perturbations in DNA replication. However, the presence of neutropenia in individuals with *TONSL* variants is consistent with its role in repairing damaged replication forks.

Taken together, the findings indicate that the cellular functions of TONSL are essential for cellular viability and that hypomorphic variants in *TONSL* have a deleterious impact at multiple stages of embryonic and postnatal development, particularly during skeletal development. Although the underlying reason for the clinical heterogeneity arising from partial loss of TONSL function is unknown, further identification of additional affected individuals will allow us to define the full extent to which variants in this gene affect clinical presentation.

Supplemental Data

Supplemental Data include four figures and five tables and can be found with this article online at https://doi.org/10.1016/j.ajhg.2019.01.007.

Consortia

The Undiagnosed Diseases Network co-investigators are David R. Adams, Aaron Aday, Mercedes E. Alejandro, Patrick Allard, Euan A. Ashley, Mahshid S. Azamian, Carlos A. Bacino, Eva Baker, Ashok Balasubramanyam, Hayk Barseghyan, Gabriel F. Batzli, Alan H. Beggs, Babak Behnam, Hugo J. Bellen, Jonathan A. Bernstein, Gerard T. Berry, Anna Bican, David P. Bick, Camille L. Birch, Devon Bonner, Braden E. Boone, Bret L. Bostwick, Lauren C. Briere, Elly Brokamp, Donna M. Brown, Matthew Brush, Elizabeth A. Burke, Lindsay C. Burrage, Manish J. Butte, Shan Chen, Gary D. Clark, Terra R. Coakley, Joy D. Cogan, Heather A. Colley, Cynthia M. Cooper, Heidi Cope, William J. Craigen, Precilla D'Souza, Mariska Davids, Jean M. Davidson, Jyoti G. Dayal, Esteban C. Dell'Angelica, Shweta U. Dhar, Katrina M. Dipple, Laurel A. Donnell-Fink, Naghmeh Dorrani, Daniel C. Dorset, Emilie D. Douine, David D. Draper, Annika M. Dries, Laura Duncan, David J. Eckstein, Lisa T. Emrick, Christine M. Eng, Gregory M. Enns, Ascia Eskin, Cecilia Esteves, Tyra Estwick, Liliana Fernandez, Carlos Ferreira, Elizabeth L. Fieg, Paul G. Fisher, Brent L. Fogel, Noah D. Friedman, William A. Gahl, Emily Glanton, Rena A. Godfrey, Alica M. Goldman, David B. Goldstein, Sarah E. Gould, Jean-Philippe F. Gourdine, Catherine A. Groden, Andrea L. Gropman, Melissa Haendel, Rizwan

Hamid, Neil A. Hanchard, Frances High, Ingrid A. Holm, Jason Hom, Ellen M. Howerton, Yong Huang, Fariha Jamal, Yong-hui Jiang, Jean M. Johnston, Angela L. Jones, Lefkothea Karaviti, David M. Koeller, Isaac S. Kohane, Jennefer N. Kohler, Donna M. Krasnewich, Susan Korrick, Mary Koziura, Joel B. Krier, Jennifer E. Kyle, Seema R. Lalani, C. Christopher Lau, Jozef Lazar, Kimberly LeBlanc, Brendan H. Lee, Hane Lee, Shawn E. Levy, Richard A. Lewis, Sharyn A. Lincoln, Sandra K. Loo, Joseph Loscalzo, Richard L. Maas, Ellen F. Macnamara, Calum A. MacRae, Valerie V. Maduro, Marta M. Majcherska, May Christine V. Malicdan, Laura A. Mamounas, Teri A. Manolio, Thomas C. Markello, Ronit Marom, Martin G. Martin, Julian A. Martínez-Agosto, Shruti Marwaha, Thomas May, Allyn McConkie-Rosell, Colleen E. McCormack, Alexa T. McCray, Jason D. Merker, Thomas O. Metz, Matthew Might, Paolo M. Moretti, Marie Morimoto, John J. Mulvihill, David R. Murdock, Jennifer L. Murphy, Donna M. Muzny, Michele E. Nehrebecky, Stan F. Nelson, J. Scott Newberry, John H. Newman, Sarah K. Nicholas, Donna Novacic, Jordan S. Orange, James P. Orengo, J. Carl Pallais, Christina GS. Palmer, Jeanette C. Papp, Neil H. Parker, Loren DM. Pena, John A. Phillips III, Jennifer E. Posey, John H. Postlethwait, Lorraine Potocki, Barbara N. Pusey, Genecee Renteria, Chloe M. Reuter, Lynette Rives, Amy K. Robertson, Lance H. Rodan, Jill A. Rosenfeld, Jacinda B. Sampson, Susan L. Samson, Kelly Schoch, Daryl A. Scott, Lisa Shakachite, Prashant Sharma, Vandana Shashi, Rebecca Signer, Edwin K. Silverman, Janet S. Sinsheimer, Kevin S. Smith, Rebecca C. Spillmann, Joan M. Stoler, Nicholas Stong, Jennifer A. Sullivan, David A. Sweetser, Queenie K.-G. Tan, Cynthia J. Tifft, Camilo Toro, Alyssa A. Tran, Tiina K. Urv, Eric Vilain, Tiphanie P. Vogel, Daryl M. Waggott, Colleen E. Wahl, Nicole M. Walley, Chris A. Walsh, Melissa Walker, Jijun Wan, Michael F. Wangler, Patricia A. Ward, Katrina M. Waters, Bobbie-Jo M. Webb-Robertson, Monte Westerfield, Matthew T. Wheeler, Anastasia L. Wise, Lynne A. Wolfe, Elizabeth A. Worthey, Shinya Yamamoto, John Yang, Yaping Yang, Amanda J. Yoon, Guoyun Yu, Diane B. Zastrow, Chunli Zhao, and Allison Zheng.

Acknowledgments

We sincerely thank the subjects and their families for participation. We thank Xiangli Yang, Alyssa Tran, Mercedes Alejandro, Brian Dawson, David Murdock, and Huan-Chang Zeng for their technical assistance. We would also like to thank Daniel Durocher, Peter Cejka, and John Rouse for kindly gifting their anti-TONSL and anti-MMS22L antibodies and expression plasmids, and to thank Yonghwan Kim for the lentiviral construct expressing Flag-*TONSL*. This work was supported by National Institutes of Health (NIH) grants U01HG007709 (B.L.), UM1HG006348 (A.B., M.D., and J.D.H.), U54NS093793 (J.P., J.W., and M.W.), U54HG006493 (M.B.), and R01AI120989 (J.S.O.); University of Utah Pathology Departmental Funds (C.C.); Associated Regional and University Pathologists (ARUP) Laboratories Roberts Memorial Fund Research Award (C.C.); NIH grant K08DK106453 (L.C.B.); and a Career Award for Medical Scientists from the Burroughs Wellcome Fund (L.C.B.). In addition, funding was received from the NIH National Institute of General Medical Sciences (NIGMS) grant T32GM007526 to B.L. and the NIH/Eunice Kennedy Shriver National Institute of Child Health and Human Development (NICHD) grant U54HD083092 for the Baylor College of Medicine Intellectual and Developmental Disabilities Research Center (IDDRC); and from the Canadian Institutes of Health Research (CIHR), the Fonds de Recherche du Québec - Santé (FRQS), and the Quebec Network for Oral and Bone Health Research (RSBO) to P.M.C. to study rare skeletal dysplasias. J.J.R. and G.S.S. are funded by a Cancer Research UK (CR-UK) programme grant (C17183/A23303) and the University of Birmingham. M.R.H. is funded by a Medical Research Council (MRC) Career Development Fellowship (MR/P009085/1) and the University of Birmingham. A.P.J. is supported by the MRC UK (grant U127580972) and the European Research Council (ERC) through the European Union's Horizon 2020 research and innovation program ERC Advanced Grant (grant agreement No: 788093). Support for D.H.C. and D.K. was provided in part by NIH Awards R01AR062651 and R01AR066124. The "Cell Line and DNA Biobank from Patients Affected by Genetic Diseases," a member of the Telethon Network of Genetic Biobanks (project no. GTB18001) funded by Telethon Italy, provided us with specimens for subject P11. Support for D.R.B. was provided by the São Paulo Research Foundation (FAPESP) grant 2015/21783-9/CEPID 2013/08028-1; CNPq 304130/2016-8. See Supplemental Acknowledgments for consortium details.

Declaration of Interests

The Department of Molecular and Human Genetics at Baylor College of Medicine receives financial support from Baylor Genetics. Dr. Brendan Lee serves on the Board of Directors of Baylor Genetics and chairs its Scientific Advisory Board but receives no personal income from these positions.

Received: August 10, 2018
Accepted: January 17, 2019
Published: February 14, 2019

Web Resources

1000 Genomes Project, http://browser.1000genomes.org
ClinVar, https://www.ncbi.nlm.nih.gov/clinvar/
CADD, https://cadd.gs.washington.edu/
Codified Genomics, https://codifiedgenomics.com/
dbSNP, https://www.ncbi.nlm.nih.gov/projects/SNP/
ExAC Database, http://exac.broadinstitute.org/
gnomAD, http://gnomad.broadinstitute.org/
GTEX Portal, https://gtexportal.org/home/
HGSC Mercury Analysis Pipeline, https://www.hgsc.bcm.edu/software/mercury
HGMD, http://www.hgmd.cf.ac.uk/ac/index.php
Human Splice Finder 3.1, http://www.umd.be/HSF3/
KOMP2, http://www.mousephenotype.org/data/genes
Mercury Pipeline, https://www.hgsc.bcm.edu/software/mercury
Mutation Taster, http://www.mutationtaster.org/
OMIM, http://www.omim.org/
PolyPhen-2, http://genetics.bwh.harvard.edu/pph2/
Sift, http://sift.jcvi.org
ZiFiT Targeter Software, http://zifit.partners.org/ZiFiT/

References

1. Fanconi, S., Issler, C., Giedion, A., and Prader, A. (1983). The SPONASTRIME dysplasia: Familial short-limb dwarfism with saddle nose, spinal alterations and metaphyseal striation. Report of 4 siblings. Helv. Paediatr. Acta *38*, 267–280.
2. Langer, L.O., Jr., Beals, R.K., LaFranchi, S., Scott, C.I., Jr., and Sockalosky, J.J. (1996). Sponastrime dysplasia: Five new cases

and review of nine previously published cases. Am. J. Med. Genet. *63*, 20–27.
3. Masuno, M., Nishimura, G., Adachi, M., Hotsubo, T., Tachibana, K., Makita, Y., Imaizumi, K., and Kuroki, Y. (1996). SPONASTRIME dysplasia: Report on a female patient with severe skeletal changes. Am. J. Med. Genet. *66*, 429–432.
4. Cooper, H.A., Crowe, J., and Butler, M.G. (2000). SPONASTRIME dysplasia: Report of an 11-year-old boy and review of the literature. Am. J. Med. Genet. *92*, 33–39.
5. Umpaichitra, V., Wallerstein, R., and Castells, S. (2002). Sponastrime dysplasia with abnormal urinary glycosaminoglycans and growth hormone unresponsiveness. Clin. Dysmorphol. *11*, 53–56.
6. Lachman, R.S., Stoss, H., and Spranger, J. (1989). Sponastrime dysplasia. A radiologic-pathologic correlation. Pediatr. Radiol. *19*, 417–424.
7. Gripp, K.W., Johnson, C., Scott, C.I., Jr., Nicholson, L., Bober, M., Butler, M.G., Shaw, L., and Gorlin, R.J. (2008). Expanding the phenotype of SPONASTRIME dysplasia to include short dental roots, hypogammaglobulinemia, and cataracts. Am. J. Med. Genet. A. *146A*, 468–473.
8. Offiah, A.C., Lees, M., Winter, R.M., and Hall, C.M. (2001). Sponastrime dysplasia: Presentation in infancy. J. Med. Genet. *38*, 889–893.
9. Nishimura, G., Mikawa, M., and Fukushima, Y. (1998). Another observation of Langer-type sponastrime dysplasia variant. Am. J. Med. Genet. *80*, 288–290.
10. Langer, L.O., Jr., Beals, R.K., and Scott, C.I., Jr. (1997). Sponastrime dysplasia: Diagnostic criteria based on five new and six previously published cases. Pediatr. Radiol. *27*, 409–414.
11. Filocamo, M.a. (2014). Cell line and DNA biobank from patients affected by genetic diseases (Open Journal of Bioresources).
12. Bainbridge, M.N., Wang, M., Wu, Y., Newsham, I., Muzny, D.M., Jefferies, J.L., Albert, T.J., Burgess, D.L., and Gibbs, R.A. (2011). Targeted enrichment beyond the consensus coding DNA sequence exome reveals exons with higher variant densities. Genome Biol. *12*, R68.
13. Challis, D., Yu, J., Evani, U.S., Jackson, A.R., Paithankar, S., Coarfa, C., Milosavljevic, A., Gibbs, R.A., and Yu, F. (2012). An integrative variant analysis suite for whole exome next-generation sequencing data. BMC Bioinformatics *13*, 8.
14. Reid, J.G., Carroll, A., Veeraraghavan, N., Dahdouli, M., Sundquist, A., English, A., Bainbridge, M., White, S., Salerno, W., Buhay, C., et al. (2014). Launching genomics into the cloud: Deployment of Mercury, a next generation sequence analysis pipeline. BMC Bioinformatics *15*, 30.
15. Li, H., and Durbin, R. (2010). Fast and accurate long-read alignment with Burrows-Wheeler transform. Bioinformatics *26*, 589–595.
16. McKenna, A., Hanna, M., Banks, E., Sivachenko, A., Cibulskis, K., Kernytsky, A., Garimella, K., Altshuler, D., Gabriel, S., Daly, M., and DePristo, M.A. (2010). The Genome Analysis Toolkit: A MapReduce framework for analyzing next-generation DNA sequencing data. Genome Res. *20*, 1297–1303.
17. Li, H., Handsaker, B., Wysoker, A., Fennell, T., Ruan, J., Homer, N., Marth, G., Abecasis, G., Durbin, R.; and 1000 Genome Project Data Processing Subgroup (2009). The Sequence Alignment/Map format and SAMtools. Bioinformatics *25*, 2078–2079.
18. Kumar, P., Henikoff, S., and Ng, P.C. (2009). Predicting the effects of coding non-synonymous variants on protein function using the SIFT algorithm. Nat. Protoc. *4*, 1073–1081.
19. Adzhubei, I.A., Schmidt, S., Peshkin, L., Ramensky, V.E., Gerasimova, A., Bork, P., Kondrashov, A.S., and Sunyaev, S.R. (2010). A method and server for predicting damaging missense mutations. Nat. Methods *7*, 248–249.
20. Schwarz, J.M., Cooper, D.N., Schuelke, M., and Seelow, D. (2014). MutationTaster2: Mutation prediction for the deep-sequencing age. Nat. Methods *11*, 361–362.
21. Reynolds, J.J., Bicknell, L.S., Carroll, P., Higgs, M.R., Shaheen, R., Murray, J.E., Papadopoulos, D.K., Leitch, A., Murina, O., Tarnauskaitė, Ž., et al. (2017). Mutations in DONSON disrupt replication fork stability and cause microcephalic dwarfism. Nat. Genet. *49*, 537–549.
22. Yang, Y., Muzny, D.M., Xia, F., Niu, Z., Person, R., Ding, Y., Ward, P., Braxton, A., Wang, M., Buhay, C., et al. (2014). Molecular findings among patients referred for clinical whole-exome sequencing. JAMA *312*, 1870–1879.
23. Sukenik Halevy, R., Chien, H.C., Heinz, B., Bamshad, M.J., Nickerson, D.A., Kircher, M., Ahituv, N.; and University of Washington Center for Mendelian Genomics (2018). Mutations in the fourth β-propeller domain of LRP4 are associated with isolated syndactyly with fusion of the third and fourth fingers. Hum. Mutat. *39*, 811–815.
24. Lopes, F., Miguet, M., Mucha, B.E., Gauthier, J., Saillour, V., Nguyen, C.E., Vanasse, M., Ellezam, B., Michaud, J.L., Soucy, J.F., and Campeau, P.M. (2018). MYOD1 involvement in myopathy. Eur. J. Neurol. *25*, e123–e124.
25. Hodgkins, A., Farne, A., Perera, S., Grego, T., Parry-Smith, D.J., Skarnes, W.C., and Iyer, V. (2015). WGE: A CRISPR database for genome engineering. Bioinformatics *31*, 3078–3080.
26. Bassett, A.R., Tibbit, C., Ponting, C.P., and Liu, J.L. (2013). Highly efficient targeted mutagenesis of Drosophila with the CRISPR/Cas9 system. Cell Rep. *4*, 220–228.
27. Westerfield, M. (2007). The zebrafish book: A guide for the laboratory use of zebrafish (Danio rerio) (The University of Oregon Press).
28. Renshaw, S.A., Loynes, C.A., Trushell, D.M., Elworthy, S., Ingham, P.W., and Whyte, M.K. (2006). A transgenic zebrafish model of neutrophilic inflammation. Blood *108*, 3976–3978.
29. Liu, D., Wang, Z., Xiao, A., Zhang, Y., Li, W., Zu, Y., Yao, S., Lin, S., and Zhang, B. (2014). Efficient gene targeting in zebrafish mediated by a zebrafish-codon-optimized cas9 and evaluation of off-targeting effect. J Genet Genomics *41*, 43–46.
30. Walker, M.B., and Kimmel, C.B. (2007). A two-color acid-free cartilage and bone stain for zebrafish larvae. Biotech Histochem. *82*, 23–28.
31. Stewart, G.S., Maser, R.S., Stankovic, T., Bressan, D.A., Kaplan, M.I., Jaspers, N.G., Raams, A., Byrd, P.J., Petrini, J.H., and Taylor, A.M. (1999). The DNA double-strand break repair gene hMRE11 is mutated in individuals with an ataxia-telangiectasia-like disorder. Cell *99*, 577–587.
32. O'Donnell, L., Panier, S., Wildenhain, J., Tkach, J.M., Al-Hakim, A., Landry, M.C., Escribano-Diaz, C., Szilard, R.K., Young, J.T., Munro, M., et al. (2010). The MMS22L-TONSL complex mediates recovery from replication stress and homologous recombination. Mol. Cell *40*, 619–631.
33. Sobreira, N., Schiettecatte, F., Valle, D., and Hamosh, A. (2015). GeneMatcher: A matching tool for connecting investigators with an interest in the same gene. Hum. Mutat. *36*, 928–930.
34. Kircher, M., Witten, D.M., Jain, P., O'Roak, B.J., Cooper, G.M., and Shendure, J. (2014). A general framework for estimating

the relative pathogenicity of human genetic variants. Nat. Genet. *46*, 310–315.
35. Szafranski, P., Karolak, J.A., Lanza, D., Gajecka, M., Heaney, J., and Stankiewicz, P. (2017). CRISPR/Cas9-mediated deletion of lncRNA Gm26878 in the distant Foxf1 enhancer region. Mamm. Genome *28*, 275–282.
36. Lanza, D.G., Gaspero, A., Lorenzo, I., Liao, L., Zheng, P., Wang, Y., Deng, Y., Cheng, C., Zhang, C., Seavitt, J.R., et al. (2018). Comparative analysis of single-stranded DNA donors to generate conditional null mouse alleles. BMC Biol. *16*, 69.
37. O'Connell, B.C., Adamson, B., Lydeard, J.R., Sowa, M.E., Ciccia, A., Bredemeyer, A.L., Schlabach, M., Gygi, S.P., Elledge, S.J., and Harper, J.W. (2010). A genome-wide camptothecin sensitivity screen identifies a mammalian MMS22L-NFKBIL2 complex required for genomic stability. Mol. Cell *40*, 645–657.
38. Duro, E., Lundin, C., Ask, K., Sanchez-Pulido, L., MacArtney, T.J., Toth, R., Ponting, C.P., Groth, A., Helleday, T., and Rouse, J. (2010). Identification of the MMS22L-TONSL complex that promotes homologous recombination. Mol. Cell *40*, 632–644.
39. Piwko, W., Olma, M.H., Held, M., Bianco, J.N., Pedrioli, P.G., Hofmann, K., Pasero, P., Gerlich, D.W., and Peter, M. (2010). RNAi-based screening identifies the Mms22L-Nfkbil2 complex as a novel regulator of DNA replication in human cells. EMBO J. *29*, 4210–4222.
40. Piwko, W., Mlejnkova, L.J., Mutreja, K., Ranjha, L., Stafa, D., Smirnov, A., Brodersen, M.M., Zellweger, R., Sturzenegger, A., Janscak, P., et al. (2016). The MMS22L-TONSL heterodimer directly promotes RAD51-dependent recombination upon replication stress. EMBO J. *35*, 2584–2601.
41. Técher, H., Koundrioukoff, S., Azar, D., Wilhelm, T., Carignon, S., Brison, O., Debatisse, M., and Le Tallec, B. (2013). Replication dynamics: Biases and robustness of DNA fiber analysis. J. Mol. Biol. *425*, 4845–4855.
42. Nieminuszczy, J., Schwab, R.A., and Niedzwiedz, W. (2016). The DNA fibre technique - tracking helicases at work. Methods *108*, 92–98.
43. Boerkoel, C.F., Takashima, H., John, J., Yan, J., Stankiewicz, P., Rosenbarker, L., André, J.L., Bogdanovic, R., Burguet, A., Cockfield, S., et al. (2002). Mutant chromatin remodeling protein SMARCAL1 causes Schimke immuno-osseous dysplasia. Nat. Genet. *30*, 215–220.
44. Mo, D., Zhao, Y., and Balajee, A.S. (2018). Human RecQL4 helicase plays multifaceted roles in the genomic stability of normal and cancer cells. Cancer Lett. *413*, 1–10.
45. Harley, M.E., Murina, O., Leitch, A., Higgs, M.R., Bicknell, L.S., Yigit, G., Blackford, A.N., Zlatanou, A., Mackenzie, K.J., Reddy, K., et al. (2016). TRAIP promotes DNA damage response during genome replication and is mutated in primordial dwarfism. Nat. Genet. *48*, 36–43.
46. Saredi, G., Huang, H., Hammond, C.M., Alabert, C., Bekker-Jensen, S., Forne, I., Reverón-Gómez, N., Foster, B.M., Mlejnkova, L., Bartke, T., et al. (2016). H4K20me0 marks post-replicative chromatin and recruits the TONSL–MMS22L DNA repair complex. Nature *534*, 714–718.
47. Campos, E.I., Smits, A.H., Kang, Y.H., Landry, S., Escobar, T.M., Nayak, S., Ueberheide, B.M., Durocher, D., Vermeulen, M., Hurwitz, J., and Reinberg, D. (2015). Analysis of the histone H3.1 interactome: A suitable chaperone for the right event. Mol. Cell *60*, 697–709.
48. Wang, A.T., Kim, T., Wagner, J.E., Conti, B.A., Lach, F.P., Huang, A.L., Molina, H., Sanborn, E.M., Zierhut, H., Cornes, B.K., et al. (2015). A dominant mutation in human RAD51 reveals its function in DNA interstrand crosslink repair independent of homologous recombination. Mol. Cell *59*, 478–490.
49. Schlacher, K., Christ, N., Siaud, N., Egashira, A., Wu, H., and Jasin, M. (2011). Double-strand break repair-independent role for BRCA2 in blocking stalled replication fork degradation by MRE11. Cell *145*, 529–542.
50. Huang, T.H., Fowler, F., Chen, C.C., Shen, Z.J., Sleckman, B., and Tyler, J.K. (2018). The histone chaperones ASF1 and CAF-1 promote MMS22L-TONSL-Mediated Rad51 loading onto ssDNA during homologous recombination in human cells. MolCell *69*, 879–892.e5.
51. Hunter, K.B., Lücke, T., Spranger, J., Smithson, S.F., Alpay, H., André, J.L., Asakura, Y., Bogdanovic, R., Bonneau, D., Cairns, R., et al. (2010). Schimke immunoosseous dysplasia: Defining skeletal features. Eur. J. Pediatr. *169*, 801–811.
52. Consortium, G.T.; and GTEx Consortium (2013). The Genotype-Tissue Expression (GTEx) project. Nat. Genet. *45*, 580–585.
53. Morio, T. (2017). Recent advances in the study of immunodeficiency and DNA damage response. Int. J. Hematol. *106*, 357–365.
54. Cottineau, J., Kottemann, M.C., Lach, F.P., Kang, Y.H., Vély, F., Deenick, E.K., Lazarov, T., Gineau, L., Wang, Y., Farina, A., et al. (2017). Inherited GINS1 deficiency underlies growth retardation along with neutropenia and NK cell deficiency. J. Clin. Invest. *127*, 1991–2006.
55. Jian, X., Boerwinkle, E., and Liu, X. (2014). In silico prediction of splice-altering single nucleotide variants in the human genome. Nucleic Acids Res. *42*, 13534–13544.
56. Desmet, F.O., Hamroun, D., Lalande, M., Collod-Béroud, G., Claustres, M., and Béroud, C. (2009). Human Splicing Finder: An online bioinformatics tool to predict splicing signals. Nucleic Acids Res. *37*, e67.